Chronic cholinergic imbalances promote brain diffusion and transport abnormalities

Eran Meshorer,*[,1,2] Inbal E. Biton,[†,1] Yoram Ben-Shaul,*[,3] Shani Ben-Ari,* Yaniv Assaf,[‡] Hermona Soreq,*[,4] and Yoram Cohen[†]

*Department of Biological Chemistry and Israel Center for Neuronal Computation, The Hebrew University of Jerusalem, Jerusalem, Israel; [†]School of Chemistry, The Raymond and Beverly Sackler Faculty of Exact Sciences, Tel-Aviv University, Ramat Aviv, Israel; and [‡]Tel Aviv Sourasky Medical Center, Human Brain Imaging Unit, The Wohl Institute for Advanced Imaging, Tel Aviv, Israel

ABSTRACT **Cholinergic imbalances occur after traumatic effects and in the initial stages of neurodegenerative diseases, but their long-lasting effects remained largely unexplained. To address this, we used TgS transgenic mice constitutively overexpressing synaptic acetylcholinesterase (AChE-S) and presenting a complex phenotype of progressive neurodeterioration. T_1- and T_2-weighted magnetic resonance (MR) brain images appeared similar. However, diffusion-weighted MRI showed decreased baseline water apparent diffusion coefficient in the brains of TgS animals. Furthermore, contrast-enhanced MRI after gadolinium diethylenetriaminepentaacetic acid (Gd-DTPA) injection demonstrated slower recovery of normal signals in the TgS brains than with controls. Perfusion MR imaging and difference T_1 maps calculated from pre- postcontrast T_1-weighted MR images indicated accumulation of more Gd-DTPA molecules in the TgS brains than in the parent strain, reflecting impaired blood-brain barrier (BBB) functioning in these transgenic mice. To explore the molecular mechanism(s) underlying these global phenotypes, we performed microarray analysis in the stress-controlling prefrontal cortex of TgS vs. strain-matched wild-type animals. Profound overexpression of numerous ion channels, transporters, and adhesion genes was confirmed by real time RT-PCR tests. Immunohistochemical and immunoblot analyses revealed corresponding increases in the level and cellular distributions of the chloride channel CLCN3 and the water channel AQP4, both of which contribute to BBB maintenance. Our study attributes to balanced cholinergic neurotransmission, a central role in the brain's maintenance of water diffusion and ion transport, and indicates that chronic impairments in this maintenance facilitate neurodeterioration through interference with BBB function.—Meshorer, E., Biton, I. E., Ben-Shaul, Y., Ben-Ari, S., Assaf, Y., Soreq, H., Cohen, Y. Chronic cholinergic imbalances promote brain diffusion and transport abnormalities. *FASEB J.* 19, 910–922 (2005)**

Key Words: cholinergic neurotransmission · acetylcholinesterase · blood-brain barrier · aquaporin 4

CHRONICALLY IMBALANCED cholinergic neurotransmission follows traumatic head affects (1) and accompanies neurodegenerative diseases (e.g., Alzheimer's and Parkinson's disease) (2, 3). However, it remained unclear whether imbalanced cholinergic neurotransmission may by itself lead to chronic brain damage(s) and, if it does, which molecular, cellular, and physiological pathways are involved. To approach this question, we used transgenic (TgS) mice with neuronal overexpression of synaptic acetylcholinesterase (AChE-S) of human origin (4). The TgS mouse displays a complex central and peripheral phenotype including fluctuations of brain acetylcholine (ACh) levels, elevated high affinity choline transport, accelerated stress-related neuropathology associated with progressive cognitive deterioration, and hypersensitivity to drugs and to close head injury (5). Peripheral impairments include complex neuromuscular pathologies (6); at least some of the central and peripheral malfunctioning symptoms could be corrected by anticholinesterase or antisense treatments, suppressing the excess AChE activities (6, 7). While this detailed picture largely points at a primary cholinergic imbalance due to neuronal AChE overexpression in the TgS mouse, the underlying changes in neuronal gene expression were never explored, and no integrative explanation was offered for this phenotype.

Prolonged AChE overexpression occurs in the mammalian brain under psychological stress (8), and various studies provide evidence that such stress can induce blood-brain barrier (BBB) disruption (9–12) via yet unknown mechanisms. Others contested this hypothesis (13), emphasizing the complexity of the issue.

[1] These authors contributed equally to this work.

[2] Present address: National Cancer Institute, 41 Library Dr., National Institutes of Health, Bethesda MD 20852, USA.

[3] Present address: Department of Neurobiology, Duke University Medical Center, Durham, NC 27710, USA.

[4] Correspondence: Department of Biological Chemistry and Israel Center for Neuronal Computation, The Hebrew University of Jerusalem, Jerusalem 91904, Israel. E-mail: soreq@cc.huji.ac.il

doi: 10.1096/fj.04-2957com

0892-6638/05/0019-0910 © FASEB

Viewing the TgS mouse as an appropriate model system for exploring these processes, we initiated a study of its BBB functioning in an effort to unravel the origin for the complex TgS phenotype and find out the consequences of chronic cholinergic imbalances. This study was designed to address two main questions: is BBB functioning impaired in the TgS mouse and, if so, which molecular mechanism(s) may lead to this impairment.

To answer the first question, we turned to magnetic resonance imaging (MRI). MRI is a noninvasive technique with high spatial and temporal resolution that enables repeated inspections of single live subjects. Combined use of various parameters obtained from MRI (e.g., T_1, T_2, T_2*, diffusion maps, and perfusion MRI) allows detailed characterization of brain water content and motion, as well as BBB status. For example, diffusion-weighted MRI (DWI) allows measurement of the apparent diffusion coefficient (ADC), which is markedly reduced in the acute ischemic brain (~30–40%) (14, 15). T_2 and ADC are widely used as a measure for various edema-related central nervous system (CNS) pathologies, such as ischemia (16, 17). Moreover, injection of contrast-enhancing compounds (perfusion MRI) provides a dynamic measure of BBB function (18, 19).

To link the physiological MRI measurements with the underlying molecular mechanisms and answer the second question, we used DNA microarrays. To improve the specificity of this analysis by limiting the neuronal complexity and focusing on a stress-relevant brain region, we selected the prefrontal cortex (PFC) (20). The PFC contributes substantially to cognitive and emotional functioning, both of which are disrupted under stress (21). Being densely populated with glucocorticoid receptors, the PFC participates in the regulatory response to stress of the hypothalamus-pituitary-adrenal axis (22). Functional MRI demonstrated impaired PFC performance in patients with post-traumatic stress disorder (PTSD) (23) and survivors of the Tokyo subway terror attack (March 20, 1995) exposed to the poisonous anticholinesterase sarin showed reduction in gray matter volume in the medial PFC (24).

To combine our physiological and molecular studies of the consequences of chronic cholinergic abnormalities, we subjected live TgS mice to brain imaging analyses, tested their PFC gene expression using microarrays, and verified the results using molecular biology and immunohistochemistry tools. We observed reduced water ADCs and BBB abnormalities in the brain of TgS mice and found evidence supporting the involvement of specific alterations in brain channels and transporters, (e.g., CLCN3 and AQP4) in these aberrations. Our findings support the notion of causal association of primary cholinergic imbalances with transport, water diffusion, and BBB impairments and point to such brain impairments as the putative origin of progressive neurodeterioration phenotypes.

MATERIALS AND METHODS

Animals

Naïve FVB/N and TgS female mice were kept on a 12 h dark/12 h light diurnal schedule and watered/fed ad libitum. All experiments were carried out in accordance with the Animal Care and Use Committee of the Hebrew University of Jerusalem (approval # NS-03-07). Control (n=13) and transgenic (n=12) mice 35 ± 10 g in weight were anesthetized by intraperitoneal injection of a 1.0 mg/kg Domitor/75 mg/kg ketamine cocktail (Pfizer, New York, NY, USA). Before performing the perfusion MRI protocol, five control and four transgenic mice were cannulated through the vein tail, under anesthesia, using a 24G Neoflon (Becton Dickinson, Franklin Lakes, NJ, USA). For the diffusion MRI protocol, a water tube (5 mm) was positioned above the head of eight control and eight transgenic mice. Animals were positioned in a head holder for securing the mouse in the MRI coil. Chamber temperature was maintained at 37°C throughout the experiment, using a circulating water blanket. At the end of the MRI protocol, mice were injected with Antisedan (Pfizer) (5 mg/mL) to terminate the effect of the anesthesia.

Body temperature of wild-type (wt) (n=2) and transgenic (n=4) mice was measured using a chrome/alume probe (type K) connected to a TES-1310 digital thermometer (TES Electrical Electronic Corp., Taipei, Taiwan).

Magnetic resonance imaging

MRI experiments were performed on an 8.4 T spectrometer (Bruker, Rheinstetten, Germany) equipped with a minimaging accessory capable of producing pulse gradients of up to 20 gauss/cm in each direction using an in-house built surface coil of 15 × 10 mm. The first MRI protocol ("diffusion protocol") included a T_1-weighted image, T_2-weighted image, and a series of diffusion-weighted MR images. The multi-slices T_1- and T_2-weighted images (5 slices of 1.35 mm thickness with a 0.2 mm gap) were acquired using the spin echo sequence with a field of view of 2.5 × 2.5 cm, matrix dimensions of 256 × 128 (transformed into a 256×256 matrix), and two averages. The repetition and echo times (TR/TE) of the T_1- and T_2-weighted MRI images were 600/20 and 3000/50 ms, corresponding to image acquisition times of 156 s and ~13 min, respectively. The diffusion-weighted images were acquired using the stimulated echo diffusion pulse sequence with the following parameters: TR = 1800 ms, TE = 41.6 ms, δ = 8 ms, Δ = 100 ms, two averages, field of view of 2.5 × 2.5 cm, matrix dimensions of 256×128 (transformed into a 256×256 matrix), and five slices of 1.35 mm thickness with a 0.2 mm gap. The diffusion gradient strength, G, was incremented from 0 to 9.23 gauss/cm in four steps, yielding a maximal b value of 3.79×10^5 s cm^{-2}. The entire diffusion protocol was completed within 1 h.

The second MRI protocol ("perfusion protocol") included two T_1-weighted images before the gadolinium diethylenetriaminepentaacetic acid (Gd-DTPA, Magnetol, Soreq Radiopharmaceuticals, Yavne, Israel) injection, a series of gradient echo images (T_2* images) pre- and post-Gd-DTPA injection, and two T_1-weighted images after the injection of the contrast agent. T_1-weighted images were acquired with the same parameters as the T_1-weighted images in the diffusion protocol. Acquisition of postcontrast T_1-weighted MR images was initiated in all cases 11 min after Gd-DTPA injection. The series of T_2*-weighted images involved single slice (1.35 mm thick), low angle (α=~10) gradient echo MR images acquired with TR = 60 ms, TE = 15 ms, one average, a field of view of 2.5 × 2.5 cm, and matrix dimensions of 64 × 32,

transformed into 64 × 64 images. The total acquisition time per image in that series was 1 s. At least 60 gradient echo images were acquired in each study. After the 10th image, 0.42 mmol/kg of Gd-DTPA was injected through the tail vein. The first 10 images were used to obtain an average baseline image. Again, the entire protocol was completed in less than 1 h.

To measure and compare Gd-DTPA blood clearance rates, we injected the tail vein of wt (n=4) and TgS (n=4) mice with 200 nmol/kg weight of Gd-DTPA diluted in phosphate-buffered saline (PBS). Tail blood samples were withdrawn 5, 11, and 16 min postinjection, diluted 1:25 in PBS, then 1:1000 in double-distilled water, and Gd-DTPA levels were measured using Inductively Coupled Plasma Mass Spectrometer (ICP-MS, Perkin Elmer, MA, USA). Similarly, prepared blood samples from naïve mice and PBS alone served as negative controls.

Image processing

ADC maps were produced using an in-house Matlab® program (The MathWorks Inc., Natick, MA, USA). The set of diffusion-weighted images were analyzed for each pixel according to Eq. 1 (25),

$$\ln(A(TE,G_i)/A(TE,0)) = -\gamma^2\delta^2G_i^2(\Delta-\delta/3)\cdot D = -bD \quad (1)$$

where $A(TE,G_i)$ and $A(TE,0)$ are the signal intensities in the presence and absence of the diffusion gradients, D is the diffusion coefficient, γ is the gyromagnetic ratio, δ and G are the duration and amplitude of the diffusion gradient pulses, and Δ is the time interval between the leading edges of these pulses. In Eq. 1, factor b represents the total diffusion weighting and $(\Delta-\delta/3)$ is the effective diffusion time for the case of rectangular diffusion gradients. We extracted from the ADC maps the diffusion coefficients of the entire brain and of six different anatomical regions. The changes in signal intensities of the T_2*-weighted images pre- and post-Gd-DTPA injection were used to extract the relative cerebral blood volume (rCBV), relative mean transit time (rMTT), and the relative cerebral blood flow (rCBF) using Eqs. 2, 3, and 4, respectively.

$$rCBV = K\int \ln\frac{S(t)}{S_0}\,dt \quad (2)$$

$$rMTT = \frac{\int t\cdot\ln\frac{S(t)}{S_0}\,dt}{\int\cdot\ln\frac{S(t)}{S_0}\,dt} \quad (3)$$

$$rCBF = \frac{rCBV}{rMTT} \quad (4)$$

In these equations, K was assumed to be 1 and $S(t)$ and S_0 are the signal intensities in the post- and precontrast images, respectively. The ratios of the rCBV, rMTT, and rCBF values between the wt and the TgS mouse groups were then calculated. In addition, we extracted the minimal normalized signals in the brain from the curves of signal as function of time. Using the pre- and post-Gd-DTPA-injected T_1-weighted MR images, we calculated the normalized subtractions maps. Then, the percentage changes in the signal intensity of all brain pixels of both groups were computed. Data presented as means ± SD was compared using 2-tailed Student's *t test*. $P < 0.05$ was considered to be significant.

DNA microarrays

PFCs from groups of four wt and four TgS animals were dissected on ice. Total PFC RNA was extracted using the RNeasy mini kit (Qiagen, Hilden, Germany). MgU74Av2 (www.affymetrix.com) mouse microarrays were used according to MIAME (www.mged.org) as described in the Affymetrix manual (www.affymetrix.com/support/downloads/manuals/expression_s2_manual.pdf). Two independent preparations of pooled PFC RNA of wt and TgS brains (4 animals each) were hybridized to four standard Affymetrix mouse arrays (MgU74Av2) containing 12,450 different transcripts. After identical data filtering processing on the four arrays, we compared the wt vs. wt, TgS vs. TgS and the four possible combinations of wt vs. TgS profiles. Analysis involved fluidic station FS-400, MAS 5.0 software and GeneArray 2500 scanner (Affymetrix). Initial filtering procedures included an absence/presence (A/P) test, where each gene should receive at least one "P" in order to be included. Marginal (M) detection levels were counted as absent. Scatter plots were computed with the remaining genes (~6000 of 12,450). Comparison tests included increase/decrease (I/D) test, and a $\log_2$ ratio of higher than 1 (or lower than –1). To identify genes that were commonly altered in all tests, we intersected the four sets of altered genes in each of the wt vs. TgS comparisons. Only genes for which the expression was similarly altered (displaying at least 2-fold difference in expression level) in the four different comparisons were regarded as "changed." Data mining and graphs were carried out using the Spotfire program (Spotfire, Somerville, MA, USA). All raw data files were submitted to GEO (http://www.ncbi.nlm.nih.gov/geo/). Accession numbers for wt-1, TgS-1, wt-2, and TgS-2 are GPL795, GPL796, GPL797, GPL798, respectively. To identify categories over-represented among the genes that were changed in the TgS brain, we performed Gene Ontologies (GO) classification using the EASE software (26) with a P value of 0.1 (1-tailed Fisher exact probability test).

Real-time PCR

RNA template (100 ng) was used for one-step RT-PCR amplification protocol (SYBR Green I RNA amplification kit, Roche, Basel, Switzerland). Primers were designed using the LC Primer/Probe design software (Roche) and ordered from Sigma (Jerusalem, Israel). All primers are given in 5′ to 3′ direction (**Table 1**). Standard curves of varying template concentrations were generated as described (27) for each primer pair; amplification efficiency for each primer pair was calculated and used for relative quantification. Samples were normalized against α-tubulin mRNA levels, which were not altered in TgS brains. All products were electrophoresed on 1% agarose gels and sequenced for verification. If more than one clear band was detected on agarose, primers were replaced or samples omitted.

Immunohistochemistry

Brains were dissected and transferred to fresh 4% paraformaldehyde in PBS solution for 7 days fixation. Sagittal paraffin-embedded sections were deparaffinized using xylene and a descending series of ethanol dilutions in double-distilled water (DDW). Antigens were retrieved by heating for 10' in a microwave oven. Intrinsic horseradish-peroxidase (HRP) activity was quenched by immersing slides in 3% H_2O_2 for 30 min. Nonspecific binding was blocked by incubation in serum (1 h, room temp.). Primary antibodies (polyclonal goat anti-CLCN3, sc-17572; Santa Cruz Biotechnology, Santa Cruz, CA, USA; and mouse monoclonal AQP4, Serotec, Cergy

TABLE 1. *Primer sequences and corresponding GenBank accession numbers and position*[a]

Gene	Accession no.	Forward primer	Position	Reverse primer	Position
MBK1	Y00305	TCTAGCGCAGTGTACTT	2477–2493	GGCTATGCTATTGTTCATATCC	2833–2854
Kcnma1	U09383	CACGGAACTCGCTAAG	3589–3604	CGGAGTGCTGTAGCCT	3916–3931
CLCN3	AF029347	TACAGATTGTGGGCCG	1380–1395	CCACCTAAGCACGCAG	1739–1754
CLCN4	Z49916	CCGATAGGAGGTGTGC	1149–1164	CTGGCGAGTGTAGGGA	1499–1514
pNBC	AF020195	ACCCGACCCAGTTAAT	1922–1937	GTCCACGCCGACTAGG	2291–2276
SCN8	U26707	TCCGCTCCGAGTACCC	4719–4734	GTCACGCTGTCGTAAG	5105–5120
Cacng2+	AF077739	ACCGTTGGTGCTTTCG	444–459	GCCCGGAGGAAATACT	673–688
vATPase	U13837	TACATGCGTGCCCTGG	1387–1402	CTCCCGGATAATGGACC	1718–1734
Nrpln	D50086	AAGCGCAAGGCTAAGT	1947–1962	ACCGTATGTCGGGAAC	2273–2288
L1-like	X94310	GTACTTGTGCCGGGAG	3404–3419	GTATGCGCCAATAAACGAT	3835–3853
ESL-1	X84037	TCTTTGTGGACCCCGT	3176–3191	CGTTAGAGGGCGCAGT	3609–3624
α-tubulin	M13444	CAACTATGCCCGTGGT	332–347	CTCAATATCTAGGTTACGGCG	669–689

[a] MBK1, voltage-gated potassium channel; Kcnma1, calcium-activated potassium channel; CLCN3 and CLCN4, chloride channels; pNBC, pancreas sodium bicarbonate cotransporter; SCN8, voltage-gated sodium channel; Cacng2+, voltage-gated calcium channel; vATPase, vacuolar ATPase; Nrpln, Neuropilin; L1-like, L1-like a.k.a CHL1; ESL-1, E-selectin ligand 1.

Saint-Christophe, France) were used in 1:100 dilutions. Biotinylated donkey anti-goat secondary antibody (Jackson Immuno-Research, West Grove, PA, USA) was used to detect CLCN3 and HRP-anti-mouse to detect AQP4. Colorimetric enzymatic detection was done with the *Elite* ABC-VECTASTAIN kit (Vector Laboratories inc., Burlingame, CA, USA) and diaminobenzidine (DAB) nickel solution for CLCN3 or standard DAB (Sigma) detection for AQP4.

RESULTS

The human AChE-S transgene includes the proximal 586 base pairs of the authentic human *ACHE* promoter in conjunction with exon 1, intron 1, and exons 2, 3, 4, and 6 encoding for AChE-S (4) (**Fig. 1*A***). This transgene is expressed in brain neurons but not in glia or muscle (28). Brain AChE activity was found to be at least 2-fold higher in TgS mice than controls and considerably more variable among individuals than in the parent strain (Fig. 1*B*), compatible with the production of the murine stress-associated AChE variant AChR-R and variable learning and memory impairments among TgS mice (7). In preparation for the MRI experiments, we tested these animals' response to anesthesia by measuring the body temperatures of TgS mice and matched controls. These measurements yielded higher body temperatures in the transgenic mice under anesthesia (Fig. 1*C*), compatible with the fluctuating levels and altered regulation of ACh shown in the TgS brain by microdialysis (29), the impaired central responses of TgS mice to anticholinesterases (8), and their impaired circadian cycle when challenged by stress (7). Altogether, these findings suggest a pronounced yet variable cholinergic imbalance in the CNS of TgS mice.

TgS mice present altered brain diffusion processes

Diffusion-weighted MR images were taken to compare bulk MRI parameters in the TgS brains to those of matched controls. Others reported considerably higher sensitivity for the DWI approach compared with T_2-weighted MRI for the evaluation of numerous CNS pathophysiological conditions (14–16, 18, 19, 30). The imaging version of the simulated echo (diffusion sequence used for conducting DWI experiments and the formula for obtaining the diffusion coefficient (D)) from the signal decay in these experiments are shown in **Fig. 2*A***.

The T_1- (data not shown) and T_2-weighted MR

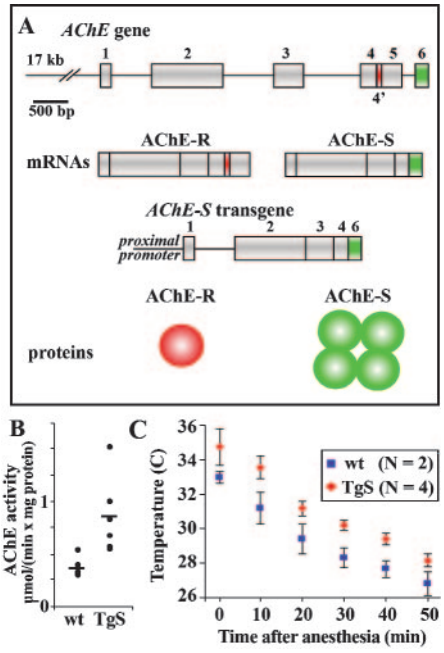

Figure 1. Transgenic overexpression and body temperature differences in the TgS mouse. *A)* Schematic illustrations of the AChE host gene, the transgene, and their major alternative products. Mice that carry the AChE-S transgene overexpress human and mouse AChE-S tetramers and murine AChE-R monomers. *B)* AChE activity in wild-type (wt) and TgS brains in μmol (min × mg protein) ± SD. *C)* Body temperature (±SD) of wt and TgS mice as a function of time from anesthesia. These findings highlight the generally impaired cholinergic phenotype of the TgS mouse.

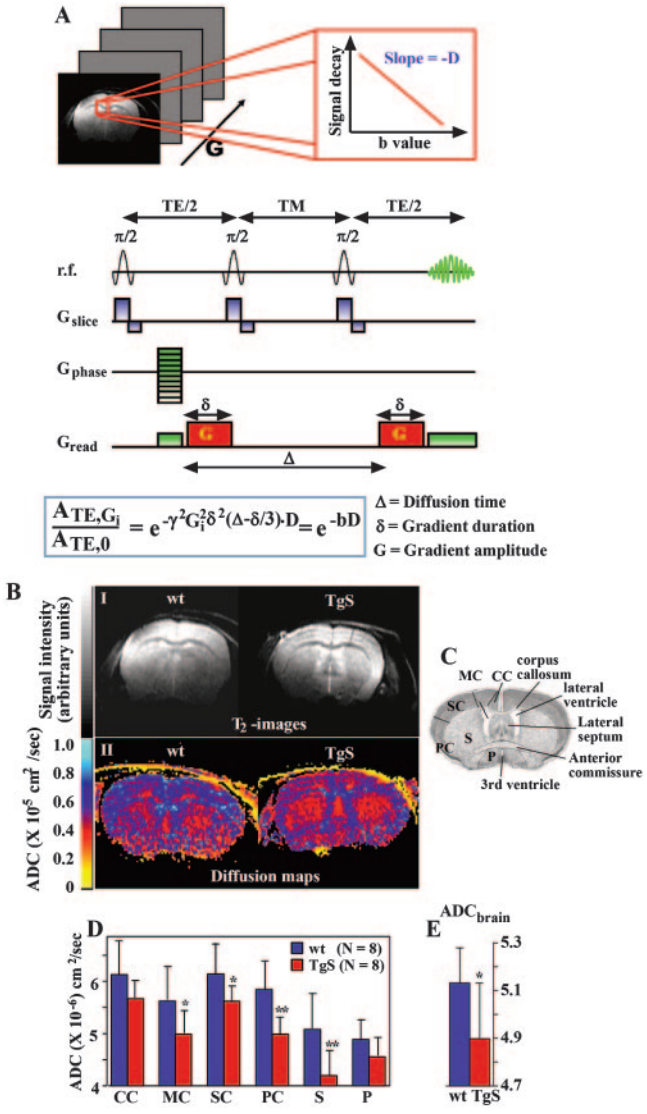

Figure 2. Altered diffusion in the TgS brain. *A)* The concept of DWI is shown on top, the stimulated echo (STE) diffusion imaging sequence is shown at the middle, and the mathematical equation underlying the signal decay in such DWI experiments is shown on the bottom. *B)* T_2-weighted images (I) and diffusion maps (II) of representative wt (left) and TgS (right) mice. *C)* Regions of interest (ROIs) used for the analysis of the diffusion coefficients (Bregma ~0 mm): CC, cingulate cortex; MC, motor cortex; SC, somatosensory cortex; PC, piriform cortex; S, striatum; P, preoptic area. *D)* Averaged diffusion coefficients (±SD) in the 6 ROIs and *E)* for the entire brain for the wt (n=8) and TgS (n=8) groups. *P < 0.05, **P < 0.01, Student's 2-tailed *t test*. These findings reflect reduced ADCs in TgS brains in 4 of 6 ROIs as well as in the brain as a whole (ADC_{brain}).

images (Fig. 2*B*, T_2 images) of the two groups of mice predictably appeared similar. This excluded the possibility of gross morphological or water content differences between brains of wt vs. TgS mice, compatible with our histological observations and earlier findings (5). In view of the sensitivity of ADC parameters for detecting CNS pathologies associated with water mobility differences, we next measured ADC values (Fig. 2*B*, diffusion maps). A statistically small decrease in the ADC values of the TgS brains was found in motor, somatosensory and piriform cortices and in the striatum (Fig. 2*C, D*, *P<0.05, **P<0.01, 2-tailed Student's *t test*). The differences observed in the cingulate cortex and the preoptic area were not significant, implying selective brain region regulation of the ADC. Average ADC values for the entire brain also showed a small but statistically significant decrease for the transgenic group (ADC_{brain}, Fig. 2*E*). Note that the lower ADC values in the brain of TgS mice could not be due to lower body temperature; rather, they occurred in spite of the higher body temperatures seen in TgS mice under anesthesia (see Fig. 1*C*, above).

Increased blood-brain barrier permeability in the TgS mouse

The decreased ADC values together with the apparent stress-related characteristics of the TgS animals further suggested altered regulation of BBB integrity. To test the physiological significance of these changes, we used contrast-enhanced MRI after i.v. injection (tail vein) of Gd-DTPA in a search for differences in perfusion rates and in BBB permeability between the two groups. The MRI protocol used in these experiments is schematized in **Fig. 3*A***. Figure 3*B* shows the normalized brain signal obtained from the T_2*-weighted images for the differ-

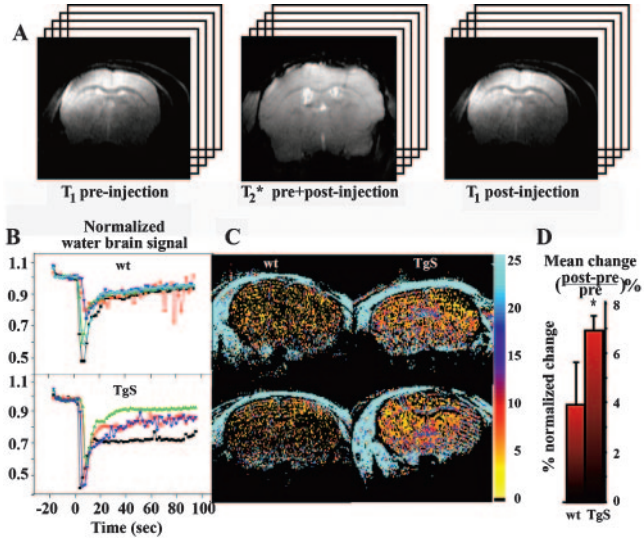

Figure 3. Promiscuous BBB in the TgS brain. *A)* The experiment included multislice T_1-weighted spin echo images before (left) and after (right) Gd-DTPA injection, as well as single slice T_2*-weighted gradient echo images taken before, during, and after the injection. *B)* Normalized ratio between the MRI signal intensity of the entire brain and a water tube (placed above the mouse head) pre- and post-Gd-DTPA injection, calculated from the T_2*-weighted images, of wt (top) and TgS (bottom) mice. *C)* T_1-weighted subtraction brain maps (100*(post-pre)/pre) of 2 representative wt (left) and TgS (right) mice. *D)* Quantification (±SD) of panel *C*. *P < 0.05, Student's 2-tailed *t test*. TgS mice show considerably slower and more variable return to precontrast baseline values as well as higher leakage of the contrast agent compared with wt.

ent mice studied pre- and post-Gd-DTPA injection. On average, signal intensities in wt mice were reduced to 65 ± 12% of the initial signal after Gd-DTPA injection, whereas signal intensities in TgS brains were reduced to 48 ± 7% of the initial signal within the same time frame ($P<0.04$). The calculated ratios of the rCBV, rMTT, and rCBF values of the wt and TgS mouse groups were 0.56 ± 0.21 ($P<0.02$), 1.03 ± 0.30 ($P>0.05$), 0.55 ± 0.20 ($P<0.01$), respectively.

Whereas wt mice responded to Gd-DTPA injection in closely similar patterns, TgS mice showed pronounced variability in this response (Fig. 3*B*). These differences matched the inter-animal differences in brain AChE activities demonstrated above (Fig. 1*B*). Moreover, for up to 100 s after Gd-DTPA injection, signal recovery in TgS brains was considerably slower than in wt mice (Fig. 3*B*). This additional test supported the notion of attenuated leakage from the brain's microvasculature of wt compared with TgS mice. Contrast-enhanced MRI thus supported the hypothesis that the BBB in wt mice was more efficient in preventing penetrance of Gd-DTPA than in the TgS mice. To ascertain that differential Gd-DTPA clearance rates from the circulation between the two strains was not causing these changes, we measured and compared blood Gd-DTPA clearance in wt and TgS animals and found no significant differences between the two ($P>0.2$, data not shown).

To test the steady-state integrity of the BBB, we have further measured T_1 images in control and TgS mice at 15 min intervals, both before and 11 min after injection of the contrast agent. Figure 3*C* shows the subtraction brain maps (100×(post-pre)/pre) of two representative wt (left) and two representative TgS mice (right). The subtraction brain maps reveal higher signals in the brains of TgS than with wt mice (Fig. 3*D*), implying that more contrast agent molecules accumulated in the TgS brains. This observation further supports the notion of weaker protection from penetrance through the BBB in TgS mice compared with wt animals. In conclusion, TgS mice displayed elevated Gd-DTPA leakage into the brain, reminiscent of the findings of others for null mice for the mdr1a gene (31). These findings represent a difference in BBB permeability between the two mice, as the GdDTPA clearance from blood was found to be similar in the two strains of mice.

Variable gene expression patterns in the TgS prefrontal cortex

To gain insight into the gene expression patterns potentially underlying the observed differences in brain water ADCs and BBB functioning, we performed DNA microarrays. Focusing on the PFC as a stress-modulating brain region, we compared gene expression profiles of TgS and gender, age and strain-matched wt controls. The two wt preparations yielded very similar profiles (**Fig. 4*A, B***), with merely five genes (~0.08% of ~ 6000 of which the detection levels were significantly above background) showing a > 2-fold detection signal difference. The two TgS microarrays

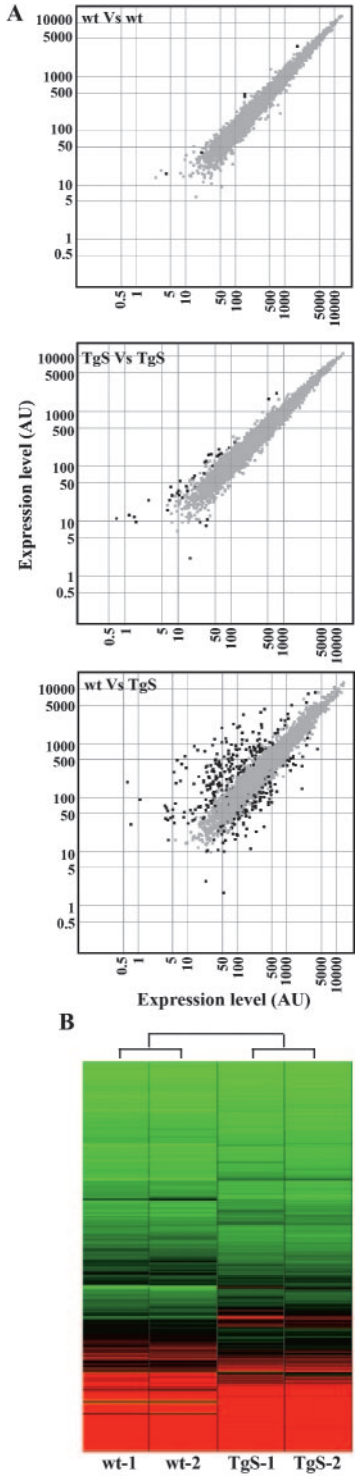

Figure 4. PFC DNA microarray analysis. *A)* Log_2 scatter plots of wt vs. wt microarrays (top), TgS Vs. TgS (middle), and wt vs. TgS (bottom). Only genes displaying higher than background intensity values are plotted (Absence/Presence Affymetrix criterion). Gray dots depict genes whose expression level was unaltered between the two tests; black dots depict genes with log ratio higher than 1. *B)* Hierarchical cluster analysis of the 4 microarrays. As expected, the 2 control, and the 2 transgenic microarrays cluster together with similar expression patterns.

displayed more limited reproducibility, with 37 genes (~0.62%) outside the 2-fold limit (Fig. 4*A*, middle). This correlated with the relatively high individual behavioral differences among TgS compared with wt animals (7), and with the higher variability in their striatal AChE activity levels (Fig. 1*B*) and body temperature under anesthesia (Fig. 1*C*). Notwithstanding, the number of genes outside the 2-fold limit was well below the expected 2% for same-sample comparisons. In sharp contrast, comparison of PFC-expressed genes in wt with TgS mice revealed over 200 genes with a > 2-fold difference between the two groups in each of the four comparisons (Fig. 4*A*, bottom). This yielded a list of 213 genes (~3.6%) (Supplementary Table S1), of which 63 are of unknown identity, producing a list of 140 genes with known annotations. The greater variability between PFC-expressed genes in the TgS mouse, and the differences between TgS and wt mRNAs are highlighted in the hierarchic clustering of the expression arrays shown in Fig. 4*B*.

Over-representation of gene classes associated with BBB features

The up-regulated genes in TgS compared with wt PFC (Supplementary Table S1) were analyzed according to their Gene Ontology annotations (http://www.geneontology.org) using EASE software (26). This analysis revealed over-represented terms in the molecular function (**Fig. 5*A***) and biological process (Fig. 5*B*) ontology branches for TgS brains (Supplementary Table S2). Two major (in terms of number of representative genes) categories with highly significant differences included transcription-related processes and ion transport/channel activity-related processes.

Within the transcriptional-related class, we identified DNA binding transcription factors, trans-acting transcriptional activators/repressors, chromatin remodeling proteins, and hormone receptors. Changes in such proteins predictably yield secondary changes downstream, resulting in differential expression of many more genes, compatible with the microarray outcome.

Within the ion transport class were included potassium, chloride (e.g., CLCN3), calcium, and sodium channels as well as a potassium channel motif kinase (Mark2), suggesting diverse changes in the transport of various ions. Increasingly recognized nonenzymatic roles of AChE include cell adhesion properties, reflected in the structural similarities between AChE and neurotactin (32, 33). Altered regulation of neuronal adhesion properties in the PFC could potentially affect cell volume and/or transport properties of the TgS brain, independently or jointly with the changes in ion transport. Compatible with this prediction, adhesion-related genes were over-represented in the TgS brain. These included neuropilin, T-cadherin, cadherin-2, contactin-1, PTEN (phosphatase and tensin homologue deleted on chromosome-10), and an L1-like

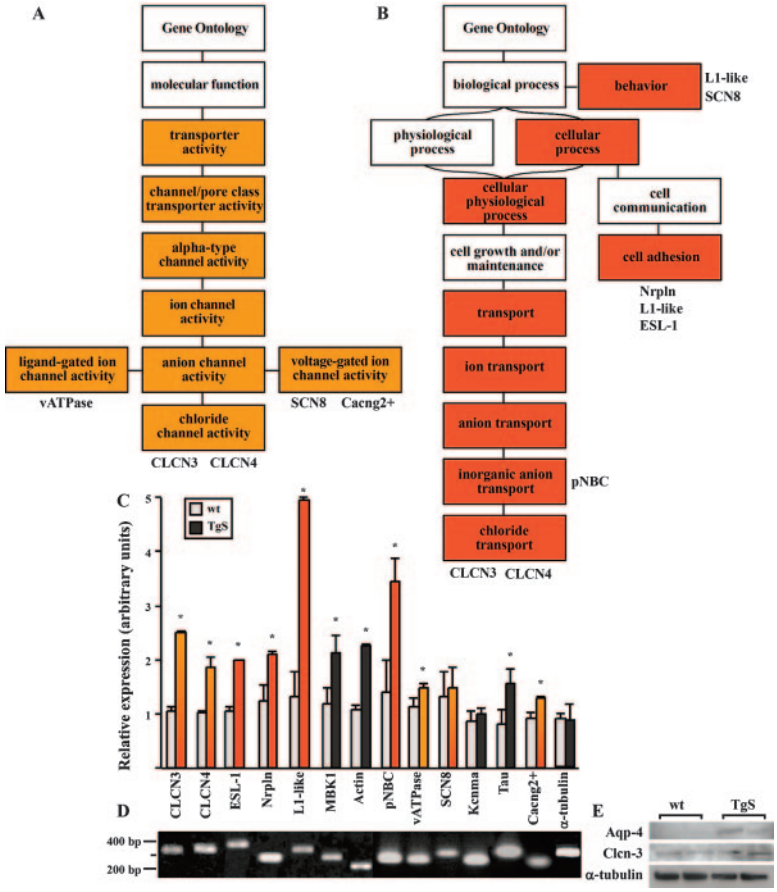

Figure 5. Gene ontology analysis and real-time RT-PCR validation of changes in PFC gene expression. *A, B)* Gene Ontology (GO) charts for 2 over-represented categories in the TgS brains: Transporter and channel activity (A) and ion transport and cell adhesion (B). Categories where genes are over-represented in the microarray tests are colored orange or red. *C)* 13 genes whose expression was altered were tested in PFC RNA extracted from at least 3 mice in each group. Shown are fold differences between TgS and wt animals ± SD. Transcript levels were compared with α-tubulin mRNA, which served as control, and showed no expression differences in the microarrays and in RT-PCR tests. $*P < 0.05$, Kruskal-Wallis test. Of the genes tested, 11 showed statistically significant elevated levels in the brains of transgenic animals, while 2 genes (SCN8 and Kcnma) displayed only mild overexpression. *D)* Amplified fragments were electrophoresed on 1% agarose gels. *E)* Western blot analysis of AQP4, CLCN3 and α-tubulin.

protein, to name a few. Compatible with the recently reported involvement of AChE-S in apoptosis (34), the TgS PFC further showed elevated transcript levels of the TNF-related cell death gene TR2L (35), the p53-related imprinted neuronal gene Peg-3 (36), and the TIA-1 gene associated with RNA metabolism and alternative splicing-related apoptosis (37), among others. Overexpression of the identified gene classes could thus be directly related to both the cholinergic (ion transport) and noncholinergic (apoptosis, adhesion) roles attributed to AChE.

Several representatives of the overexpressed channel- or adhesion-related genes were selected for real-time RT-PCR analysis. Two genes (SCN8 and Kcnma) showed no significant increase in RT-PCR, but 11 of 13 demonstrated reproducible and significant overexpression in the TgS PFC compared with wt (Fig. 5*C, D*), validating the microarray observations. Alpha-tubulin, which was selected for control based on our microarray results, remained unchanged in our real-time PCR analysis as well (Fig. 5*C, D*, right).

Cellular accumulation of ion/water controllers in the TgS brain

To more deeply explore the significance of the changes observed in the microarray analysis, we decided to focus on two specific genes: CLCN3 and AQP4. Located on synaptic and lysosomal vesicles, the voltage-gated chloride channel CLCN3 contributes to their luminal acidification (38). CLCN3 was suggested to be involved in the regulation of cell volume (39), belonging to the family of volume-sensitive organic osmolyte and anion channels (VSOACs) (40). AQP4 was shown to be involved in brain water transport (41), ischemia (42), and edema (43) as well as in the development and integrity of the BBB (44). Therefore, CLCN3 and AQP4 could both be potentially involved in the complex phenotype of the TgS mouse.

Microarray and RT-PCR analyses, which use total RNA as input, do not necessarily imply elevation of protein levels. They cannot distinguish between elevated mRNA (or protein) levels in all cells that express a certain gene or increased number of cells expressing that gene. To measure protein levels, we first used immunoblot analysis of total PFC protein extracts of wt and TgS mice for CLCN3 and AQP4. In both cases, elevated protein levels were observed (Fig. 5*E*). To explore their cellular and subcellular distribution, we immunostained the CLCN3 and AQP4 proteins in brain sections from wt and TgS mice.

CLCN3 staining was considerably higher in the TgS brain, mainly in the brainstem, with 37% increase in the number of CLCN3-positive brainstem cells ($P<0.01$, 2-tailed Student's *t test*, **Fig. 6*A, B***). Histochemical staining revealed that CLCN3 staining was observed in glia (57% of the labeled cells) and neurons (43%) in wt and TgS mice. CLCN3 distribution within wt brain cells showed cell circumference location whereas CLCN3 in TgS cells filled the entire cellular space (Fig. 6*C–E*).

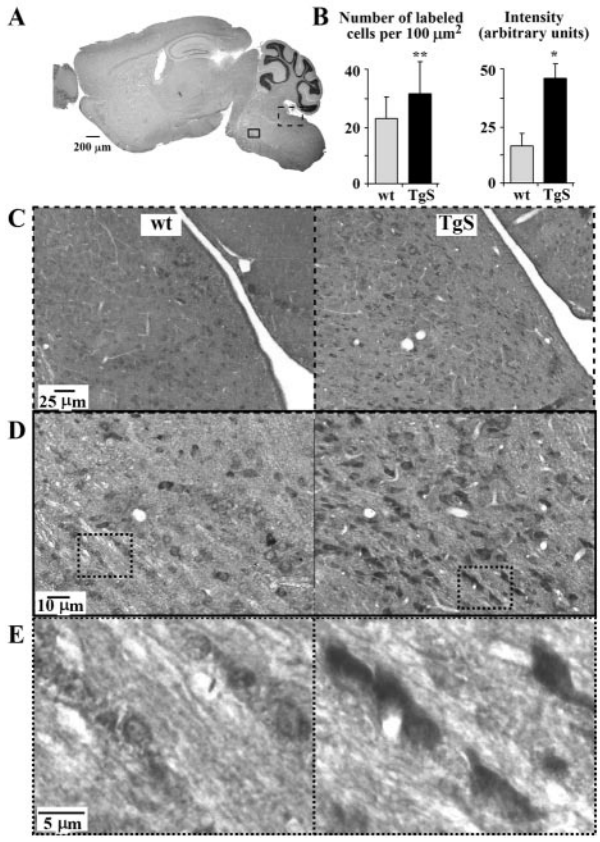

Figure 6. Increased CLCN3 expression and cell distribution in the TgS brain. *A)* CLCN3 immunolabeling in the mouse brain. *B)* CLCN3-positive cell counts/100 μm^2 ($\pm$SD, left columns), with 37% increase in number of CLCN3-positive cells in the brainstem of TgS compared with wt mice (bottom right, $P<0.01$, 2-tailed Student's *t test*). Right panel columns show quantification of CLCN3 immunostaining intensity ($\pm$SD) ($P<0.05$). *C)* Immunohistochemistry of CLCN3 in the upper right region in the brainstem (dashed frame in panel *A*) in wt (left) and TgS (right) mice. *D)* CLCN-3 immunohistochemistry in the central brainstem (rectangle in panel *A*). Details as in panel *C*. *E)* Enlargement of the dotted rectangle shown in panel *D*. Note the distinct magnification scales in each section and the subcellular distribution patterns of CLCN3 in wt and TgS cells.

Thus, the cholinergic imbalance in the TgS brain and/or the nonenzymatic features of AChE enhanced CLCN3 expression levels and modified its cellular and subcellular distribution in cells of neural and glial origin.

Staining intensity of the water channel AQP4 was significantly stronger in the brains of TgS compared with wt animals (**Fig. 7*A–D***), yet the number of labeled cells was similar (Fig. 7*B*, left). Thus, excess of AChE-S intensified AQP4 expression without altering the number of expressing cells. Most cells in the wt brain showed punctuated cytoplasmic labeling. In contrast, cells in the TgS brain's microvascular system were labeled in the cytoplasm and nucleus (Fig. 7*E, F*). Histological H&E staining revealed no differences in cell number, density, or the incidence of necrotic or apoptotic cells between wt and TgS animals (data not

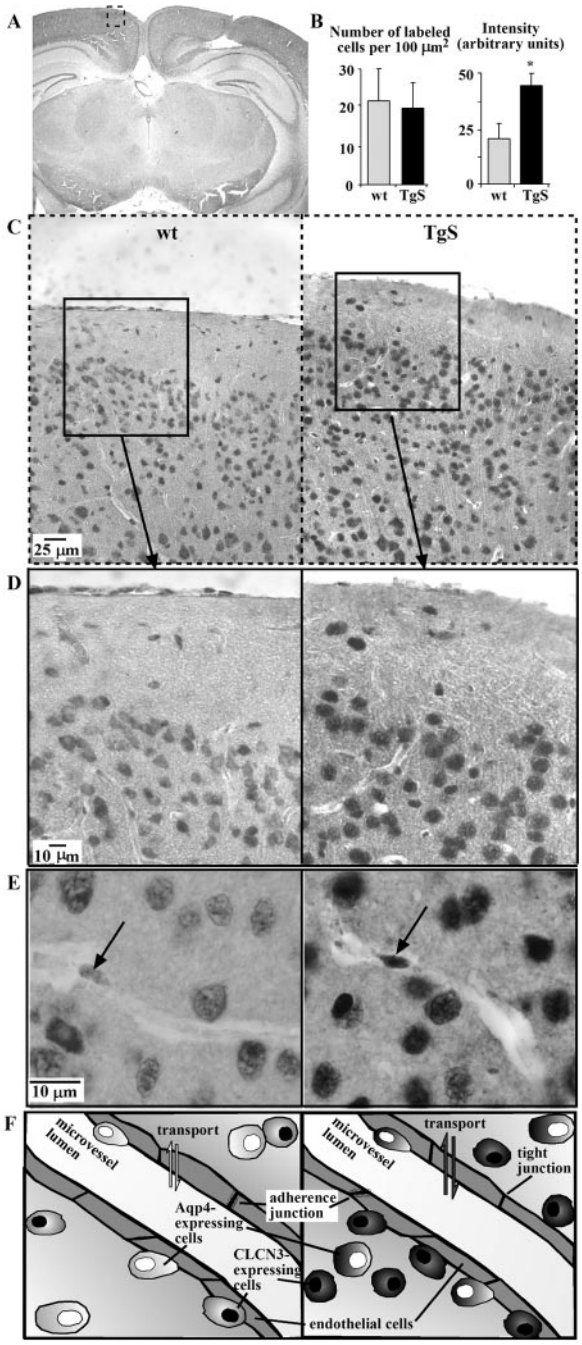

Figure 7. Enhanced AQP4 expression in the TgS brain. *A)* AQP4 immunolabeling. The analyzed area in the mouse cortex is represented schematically by a rectangle. *B)* Cell counts per 100 μm^2 ±SD for AQP4-labeled cells (left panel) or labeling intensity (arbitrary units, right panel, ±SD). Although labeling was considerably more intense in TgS animals, the number of AQP4-positive cells appeared the same in wt and TgS mice. *C)* Immunolabeling of AQP4 in wt (left) and TgS (right) mice within the rectangle shown in panel *A*. *D)* Enlargement of the framed region in panel *C*. *E)* Enhanced AQP4 expression in brain microvasculature of TgS mice. Note microvessels (arrows) surrounded by AQP4 positive cells. *F)* Schematic representation of the microvasculature of wt (left) and TgS (right) brains. Elongated endothelial cells are shown in gray surrounding the microvessel. CLCN3 (black nuclei) and AQP4-positive cells (white nuclei) are labeled. Intensity represents relative expression levels.

shown), suggesting the occurrence of functional changes but not cell death.

The association of a large number of overexpressed channels and transporters in the TgS brains including, specifically, AQP4, and BBB abnormalities, suggested the possible involvement of AQP1, since it is known to be selectively expressed in choroids plexus of the lateral ventricles (45, 46). We therefore performed immunostaining for AQP1 in wt and TgS brains, but found no significant differences in the expression levels or number of AQP1-expressing cells between the two strains (Supplementary Fig. S1).

The cholinergic imbalance, CLCN3 and AQP4 overexpression, and BBB impairments further showed spatial associations. Within the TgS brain, transgenic AChE-S and host AChE-R showed distribution patterns that mimic those of the normal brain, with particularly high expression levels in the basal nuclei and cortical periphery, respectively (**Fig. 8*A, B***). This matched the sum of the observed diffusion differences (Fig. 8*B*). Intriguingly, AQP4 and CLCN3 accumulation (Fig. 8*C*) matched these regions as well as the brain diffusion abnormalities observed in the TgS brain. While higher

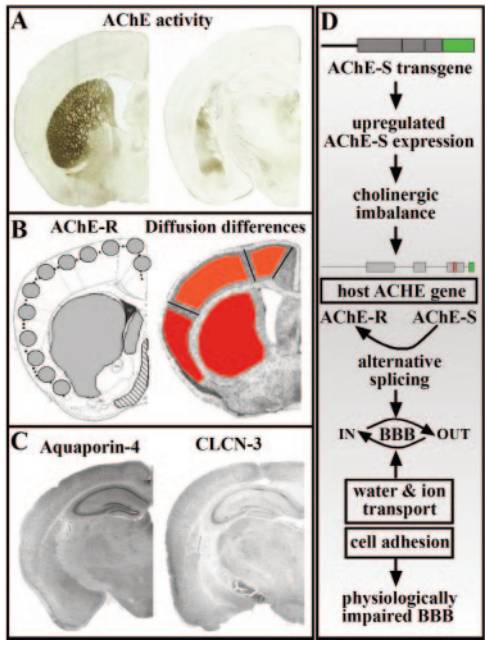

Figure 8. From AChE overexpression to impaired BBB functioning. *A)* AChE-S accumulates in brain nuclei, shown here as histochemical staining of acetylthiocholine hydrolysis in a frozen brain section (after ref 61). *B)* AChE-R labeling is seen in brain nuclei and in cortex (left; after ref 62), and diffusion differences are observed in the same regions (after Fig. 2 in this manuscript). *C)* AQP4 and CLCN3 expression in the TgS brain together match the diffusion difference maps. Note conspicuous AQP4 expression in hippocampal neurons and brain nuclei, and elevated CLCN3 levels in the piriform cortex. *D)* Putative cascade. Excess AChE-S causes cholinergic imbalance, which modifies the alternative splicing pattern of AChE mRNA transcripts and alters the expression patterns of numerous genes, changing BBB functioning, by implementing modifications in water and ion transport, cell adhesion, and additional genes.

resolution tests and different experimental approaches would be required to establish the corresponding cellular events, these similarities were compatible with the hypothesis that excess AChE-S and the resultant cholinergic imbalance and cell adhesion changes induced elevations in water and ion transport, leading to consequent BBB promiscuity (Fig. 8*D*). The differences in CLCN3 and AQP4 overexpression thus suggested causal involvement with the physiological phenotype and BBB malfunctioning of the TgS brains.

DISCUSSION

We combined in vivo MRI tests, oligonucleotide microarrays, and immunohistochemistry to explore the molecular, cellular, and physiological effects of chronic cholinergic imbalances on basic functional properties of the mammalian brain. Our findings of significant changes in the brain's diffusion and perfusion parameters strengthen the notion of alterations in water mobility and BBB integrity under cholinergic imbalances. Corresponding changes in gene expression, especially of proteins involved with adhesion and transport of water and ions, provide a plausible molecular pathway explaining the complex phenotype observed in TgS mice. Cholinergic imbalances and the diverse environmental stimuli that lead to it hence should be considered as a major cause for impaired brain diffusion and transport processes.

Lower ADC in TgS mice

The indistinguishable T_1 and T_2 images in TgS and wt mice suggest similar total brain water content. Nevertheless, the corresponding diffusion maps were significantly different for these two strains. ADC, a common parameter for assessing the motion of water in tissues, is extremely sensitive to cytotoxic edema during cerebral insults such as stroke (14–16) and is used to evaluate water motion in other CNS pathologies (17, 47). Similar to animal models of ischemia or stroke with elevated AQP4, TgS mice displayed lower baseline ADC values than their age-matched controls. As expected, the transgenic effect was less dramatic to the integrity of the brain than those of direct physical insults. Quantitative comparison of the observed ADC differences in TgS mice (~4.5%) shows a limited effect compared with that observed in ischemic stroke (~30–40%) (14–16). However, to the best of our knowledge this is the first report of baseline differences in ADC in an animal strain with transgenic overexpression of a single protein (48), highlighting the profound physiological consequences induced by the primary subtle overexpression of the AChE-S transgene.

Putative causes for the reduced ADC values

At the organismal level, lower body temperature could have caused ADC decreases. However, TgS mice presented higher body temperature than wt mice and demonstrated limited decreases in body temperature under the anesthetic conditions used in the MRI tests. The effect of brain tissue density was also considered. Richer dendritic arborisations could lead to smaller extracellular volumes and possibly higher restriction, and hence lower average ADC values. However, TgS mice suffer progressive loss of their dendritic arborisations (49). Together with the higher body temperature, this could potentially increase the ADC values, suggesting that the ADC decreases seen may in fact conceal yet larger functional discrepancies.

At the cellular level, one would expect faster motion of ions and water molecules into and out of TgS brain cells, with a possible change in cell volume regulation due to the up-regulated CLCN3 and other ion channels. In the spinal cord of TgS mice, we indeed observed increased cell volume of motoneurons (5), which might be explained by such changes. Even a subtle increase in the volume of brain cells will reciprocally reduce the extracellular space, thus restricting diffusion and leading to reduced ADC, as is the case in the ischemic brain (15).

At the molecular level, the ADC reduction observed in the brains of TgS mice might be due to the elevated mRNA and protein levels of ion and water channels, such as AQP4. AQP4 overexpression follows the course of the brain edema induced by ischemia (42) and displays an inverse correlation with ADC after ischemia (50). In dystrophin null transgenic mice with mislocalized AQP4, the decrease in ADC that normally follows edema was delayed (51). This is compatible with the findings that AQP4 null mice show delayed brain edema after water intoxication (43) and that TgS mice show exaggerated edema after head injury (5).

Transgenic effects on BBB integrity

In healthy mammals, injected contrast agents would transiently reach the brain's microvasculation system, creating a short-lasting signal change. This was indeed the case in the wt FVB/N mice, demonstrating an apparently intact BBB. However, TgS animals displayed considerable variability in the extent and duration of brain signal change after perfusion of Gd-DTPA, compatible with the assumption of variably disrupted BBB properties in TgS mice: in several of these mice, larger quantities of the injected contrast agent apparently leaked out of the vascular system into the brain tissue itself. Changes in ADC values are often, but not always, accompanied by apparent BBB disruption.

Several pieces of evidence support the assumption that reduced ADC values together with the secondary feedback responses that occurred in the TgS brain were causally related to BBB disruption. First, the up-regulated ion channels and transporters in the TgS brain likely reflect altered control over ion transport. This could be due to the cholinergic imbalance, which mimics chronic stress conditions. Second, drug penetrance into the brain of FVB/N mice was shown to

increase after confined swim stress (10); exposure to anticholinesterases, which also induces cholinergic imbalance, impairs BBB functioning (52). While this was difficult to reproduce in postmortem perfusion-based studies (13), human brain imaging demonstrated an apparent association of stress and AChE overexpression with BBB disruption (12). Recent studies further demonstrate cholinergic control over inflammatory reactions (53), which constitute an important element in BBB disruption (54). Acute stress was reported to increase BBB permeability through activation of brain mast cells (11), supporting the notion that cholinergic control is involved.

Third, modified adhesion elements, due to either AChE's nonenzymatic features or changes induced in gene expression, could change the physical composition of the BBB. Our current findings thus outline a cascade of events initiating with cholinergic imbalance, proceeding with modified gene expression, ion and water transport, and cell adhesion, and culminating in chronic BBB disruption, which in turn promotes progressive neurodeterioration.

Profound impact on PFC gene expression

PFC neurons from TgS brains showed significant differences in their gene expression patterns, compatible with the involvement of the PFC in organismal responses associated with cholinergic imbalance (e.g., psychological stress). TgS and wt PFC microarrays demonstrated >200 transcripts with expression differences. For comparison, cerebral mRNA from transgenic mice overexpressing cyclooxygenase 2, which is involved in neuronal cell cycle activity and glutamate-mediated neurotoxicity, showed altered expression of only one gene (55). The more limited variety of PFC neurons could assist in detecting subtle expression differences; nevertheless, that so many genes showed modified expression levels supports the notion that cholinergic imbalance and/or excess of AChE-S exert profound changes on numerous cellular processes. The wt and TgS mice are inbred strains, with minimal inter-animal differences to be expected. However, TgS mice showed larger variability in PFC transcripts than wt mice, suggesting experience-derived contribution in addition to their genotype differences.

Distinct responding cell types and modes of up-regulation

The cell volume regulator channel CLCN3 is expressed in more cells in the TgS than in the wt brain. The water channel AQP4, however, is expressed in higher cellular levels but in a similar number of cells in the TgS and wt mice. In both cases, glial cells showed differences, although the AChE-S transgene is expressed only in neurons (7). Therefore, the observed phenomena reflected a tissue level response to the transgenic effects. The modified AQP4 expression patterns were especially intriguing because of AQP4 involvement with focal cerebral ischemia (42), brain edema under intoxication or ischemic stroke (43), and the integrity of the BBB (44). This is compatible with TgS mice being considerably more sensitive to closed head injury than wt mice (5), and suggests their impaired BBB might have been involved.

Changes observed in the expression of ion and water channels, transporters, and adhesion-associated proteins could explain the differences in the mobility of water and ions into and out of brain cells and in BBB integrity. These effects are likely to be manifested in hierarchically higher brain organization and/or functioning levels, proposing a putative mechanistic explanation to the noninvasive in vivo brain imaging that revealed changes in water ADCs and BBB permeability.

AQP4 and CLCN3 reflect a more general alteration

Being a water channel, AQP4 is intensively expressed in the brain's microvascular epithelium; its levels increase in diseases associated with BBB disruption (56) and its absence protects the mouse brain from damages characteristic of BBB malfunctioning (43). However, AQP4 is unlikely to account for the entire TgS phenotype. Rather, multiple small effects of numerous genes, proteins, and their complex interactions are likely involved. Ion channels such as CLCN3 or CLCN4 are induced in neurons and glia alike, probably magnifying neuron-glia interactions that are pivotal elements of BBB regulation (54). Adhesion proteins such as selectin, neuropilin, contactin, and PTEN, also known to increase in the ischemic brain (57–60), probably contribute as well. That subtle changes in the brain's cholinergic balance suffice to disrupt basic transport processes supports the notion that this balance is an essential prerequisite for BBB maintenance.

Molecular and cellular basis of the TgS phenotype

By overexpressing transgenic synaptic AChE-S and host AChE-R, the TgS mouse represents a situation where stress-induced transcriptional activation occurred but did not involve the alternative splicing shift that limits AChE-S excess in the healthy mammalian brain (8). This would result in suppressed cholinergic signals into cholinoceptive neurons, unlike normal brain responses where soluble AChE-R limits acetylcholine levels throughout the brain, ameliorating cholinergic excitation of noncholinergic neurons carrying acetylcholine receptors (e.g., GABAergic, glutamatergic, and dopaminergic neurons). Our microarray tests demonstrate that such AChE-S excess induces massive changes in neuronal gene expression, presumably aimed at retrieving cholinergic tone sufficient for survival. These changes would likely facilitate neuronal capacities to respond to remaining acetylcholine molecules but that further impair cell adhesion processes. Together, these suffice to interfere with the maintenance of BBB functioning, which in turn may explain the progressive accumulation of stress-associated neuropathologies in

the TgS brain and its consequent cognitive deterioration (5).

Cholinergic imbalances likely occur in patients with Alzheimer's disease or in the brain of PTSD patients; BBB maintenance, which we found to be considerably more vulnerable than previously perceived (10), thus protects the mammalian brain from neurodeterioration, but is continuously subject to attacks of environmental origin. FJ

We thank Dr. Asher Meshorer (Rehovot, Israel) for help with histology and pathology and Dr. Osnat Cohen for assistance with animal experiments. This research was supported by the Israel Science Fund (618y02), U.S. Army Medical Research and Materiel Command (DAMD 17-99-1-9547), the European Union (LSHM-CT-2003-503330) and Ester Neuroscience, Tel-Aviv (to H.S.), the German Federal Ministry of Education and Research (BMBF) within the framework of the German-Israeli Project (DIP) (to Y.C.). E.M. was an incumbent of the Hebrew University's Rector Fellowship and a Golda Meir Fellow. Y.B.-S. was supported by the Interdisciplinary Center for Neural Computation (ICNC) postdoctoral fellowship.

REFERENCES

1. Murdoch, I., Perry, E. K., Court, J. A., Graham, D. I., and Dewar, D. (1998) Cortical cholinergic dysfunction after human head injury. *J. Neurotrauma* **15,** 295–305
2. Wilson, J. T. (2003) Head injury and Alzheimer's disease. *J. Neurol. Neurosurg. Psychiatry* **74,** 841
3. Roses, A. D., and Saunders, A. (1995) Head injury, amyloid beta and Alzheimer's disease. *Nat. Med.* **1,** 603–604
4. Beeri, R., Andres, C., Lev Lehman, E., Timberg, R., Huberman, T., Shani, M., and Soreq, H. (1995) Transgenic expression of human acetylcholinesterase induces progressive cognitive deterioration in mice. *Curr. Biol.* **5,** 1063–1071
5. Soreq, H., and Seidman, S. (2001) Acetylcholinesterase—new roles for an old actor. *Nat. Rev. Neurosci.* **2,** 294–302
6. Farchi, N., Soreq, H., and Hochner, B. (2003) Chronic acetylcholinesterase overexpression induces multilevelled aberrations in mouse neuromuscular physiology. *J. Physiol. (London)* **546,** 165–173
7. Cohen, O., Erb, C., Ginzberg, D., Pollak, Y., Seidman, S., Shoham, S., Yirmiya, R., and Soreq, H. (2002) Neuronal overexpression of 'readthrough' acetylcholinesterase is associated with antisense-suppressible behavioral impairments. *Mol. Psychiatry* **7,** 874–885
8. Meshorer, E., Erb, C., Gazit, R., Pavlovsky, L., Kaufer, D., Friedman, A., Glick, D., Ben-Arie, N., and Soreq, H. (2002) Alternative splicing and neuritic mRNA translocation under long-term neuronal hypersensitivity. *Science* **295,** 508–512
9. Sharma, H. S., and Dey, P. K. (1988) EEG changes following increased blood-brain barrier permeability under long-term immobilization stress in young rats. *Neurosci. Res.* **5,** 224–239
10. Friedman, A., Kaufer, D., Shemer, J., Hendler, I., Soreq, H., and Tur Kaspa, I. (1996) Pyridostigmine brain penetration under stress enhances neuronal excitability and induces early immediate transcriptional response. *Nat. Med.* **2,** 1382–1385
11. Esposito, P., Gheorghe, D., Kandere, K., Pang, X., Connolly, R., Jacobson, S., and Theoharides, T. C. (2001) Acute stress increases permeability of the blood-brain-barrier through activation of brain mast cells. *Brain Res.* **888,** 117–127
12. Tomkins, O., Kaufer, D., Korn, A., Shelef, I., Golan, H., Reichenthal, E., Soreq, H., and Friedman, A. (2001) Frequent blood-brain barrier disruption in the human cerebral cortex. *Cell. Mol. Neurobiol.* **21,** 675–691
13. Ovadia, H., Abramsky, O., Feldman, S., and Weidenfeld, J. (2001) Evaluation of the effect of stress on the blood–brain barrier: critical role of the brain perfusion time. *Brain Res.* **905,** 21–25
14. Moseley, M. E., Cohen, Y., Mintorovitch, J., Chileuitt, L., Shimizu, H., Kucharczyk, J., Wendland, M. F., and Weinstein, P. R. (1990) Early detection of regional cerebral-ischemia in cats—comparison of diffusion-weighted and T_2-weighted Mri and spectroscopy. *Magn. Reson. Med.* **14,** 330–346
15. Yongbi, M. N., Huang, N. C., Branch, C. A., and Helpern, J. A. (1997) The application of diffusion-weighted line-scanning for the rapid assessment of water ADC changes in stroke at high magnetic fields. *NMR Biomed.* **10,** 79–86
16. Hossmann, K. A., and Hoehn-Berlage, M. (1995) Diffusion and perfusion MR-imaging of cerebral-ischemia. *Cerebrovasc. Brain Metab. Rev.* **7,** 187–217
17. Schaefer, P. W., Grant, P. E., and Gonzalez, R. G. (2000) Diffusion-weighted MR imaging of the brain. *Radiology* **217,** 331–345
18. Stark, D. D., and Bradley, W. G., Jr. (1999) *Magnetic Resonance Imaging,* Vol. I-III, Mosby, St. Louis, MO
19. Benveniste, H., and Blackband, S. (2002) MR microscopy and high resolution small animal MRI: applications in neuroscience research. *Prog. Neurobiol.* **67,** 393–420
20. Van Eden, C. G., and Buijs, R. M. (2000) Functional neuroanatomy of the prefrontal cortex: autonomic interactions. *Prog. Brain Res.* **126,** 49–62
21. Moghaddam, B. (2002) Stress activation of glutamate neurotransmission in the prefrontal cortex: implications for dopamine-associated psychiatric disorders. *Biol. Psychiatry* **51,** 775–787
22. Lupien, S. J., and Lepage, M. (2001) Stress, memory, and the hippocampus: can't live with it, can't live without it. *Behav. Brain Res.* **127,** 137–158
23. Shin, L. M., Whalen, P. J., Pitman, R. K., Bush, G., Macklin, M. L., Lasko, N. B., Orr, S. P., McInerney, S. C., and Rauch, S. L. (2001) An fMRI study of anterior cingulate function in posttraumatic stress disorder. *Biol. Psychiatry* **50,** 932–942
24. Yamasue, H., Kasai, K., Iwanami, A., Ohtani, T., Yamada, H., Abe, O., Kuroki, N., Fukuda, R., Tochigi, M., Furukawa, S., et al. (2003) Voxel-based analysis of MRI reveals anterior cingulate gray-matter volume reduction in posttraumatic stress disorder due to terrorism. *Proc. Natl. Acad. Sci. USA* **100,** 9039–9043
25. Stejskal, E. O., and Tanner, J. E. (1965) Spin diffusion measurements: Spin echoes in presence of a time-dependent field gradient. *J. Chem. Phys.* **42,** 288–292
26. Hosack, D. A., Dennis, G., Jr., Sherman, B. T., Lane, H. C., and Lempicki, R. A. (2003) Identifying biological themes within lists of genes with EASE. *Genome Biol.* **4,** R70
27. Bustin, S. A. (2000) Absolute quantification of mRNA using real-time reverse transcription polymerase chain reaction assays. *J. Mol. Endocrinol.* **25,** 169–193
28. Andres, C., Beeri, R., Friedman, A., Lev-Lehman, E., Henis, S., Timberg, R., Shani, M., and Soreq, H. (1997) Acetylcholinesterase-transgenic mice display embryonic modulations in spinal cord choline acetyltransferase and neurexin Ibeta gene expression followed by late-onset neuromotor deterioration. *Proc. Natl. Acad. Sci. USA* **94,** 8173–8178
29. Erb, C., Troost, J., Kopf, S., Schmitt, U., Loffelholz, K., Soreq, H., and Klein, J. (2001) Compensatory mechanisms enhance hippocampal acetylcholine release in transgenic mice expressing human acetylcholinesterase. *J. Neurochem.* **77,** 638–646
30. Schaeffer, E., Alder, J., Greengard, P., and Poo, M. M. (1994) Synapsin IIa accelerates functional development of neuromuscular synapses. *Proc. Natl. Acad. Sci. USA* **91,** 3882–3886
31. Schinkel, A. H., Smit, J. J., van Tellingen, O., Beijnen, J. H., Wagenaar, E., van Deemter, L., Mol, C. A., van der Valk, M. A., Robanus-Maandag, E. C., te Riele, H. P., et al. (1994) Disruption of the mouse mdr1a P-glycoprotein gene leads to a deficiency in the blood-brain barrier and to increased sensitivity to drugs. *Cell* **77,** 491–502
32. de la Escalera, S., Bockamp, E. O., Moya, F., Piovant, M., and Jimenez, F. (1990) Characterization and gene cloning of neurotactin, a *Drosophila* transmembrane protein related to cholinesterases. *EMBO J.* **9,** 3593–3601
33. Darboux, I., Barthalay, Y., Piovant, M., and Hipeau Jacquotte, R. (1996) The structure-function relationships in *Drosophila* neurotactin show that cholinesterasic domains may have adhesive properties. *EMBO J.* **15,** 4835–4843

34. Park, S. E., Kim, N. D., and Yoo, Y. H. (2004) Acetylcholinesterase plays a pivotal role in apoptosome formation. *Cancer Res.* **64,** 2652–2655
35. Cao, H., Mattison, J., Zhao, Y., Joki, N., Grasso, M., and Chang, N. S. (1996) Regulation of tumor necrosis factor-and Fas-mediated apoptotic cell death by a novel cDNA TR2L. *Biochem. Biophys. Res. Commun.* **227,** 266–272
36. Johnson, M. D., Wu, X., Aithmitti, N., and Morrison, R. S. (2002) Peg3/Pw1 is a mediator between p53 and Bax in DNA damage-induced neuronal death. *J. Biol. Chem.* **277,** 23000–23007
37. Forch, P., and Valcarcel, J. (2001) Molecular mechanisms of gene expression regulation by the apoptosis-promoting protein TIA-1. *Apoptosis* **6,** 463–468
38. Stobrawa, S. M., Breiderhoff, T., Takamori, S., Engel, D., Schweizer, M., Zdebik, A. A., Bosl, M. R., Ruether, K., Jahn, H., Draguhn, A., et al. (2001) Disruption of ClC-3, a chloride channel expressed on synaptic vesicles, leads to a loss of the hippocampus. *Neuron* **29,** 185–196
39. Arreola, J., Begenisich, T., Nehrke, K., Nguyen, H. V., Park, K., Richardson, L., Yang, B., Schutte, B. C., Lamb, F. S., and Melvin, J. E. (2002) Secretion and cell volume regulation by salivary acinar cells from mice lacking expression of the Clcn3 Cl^- channel gene. *J. Physiol. (London)* **545,** 207–216
40. Wang, G. X., Hatton, W. J., Wang, G. L., Zhong, J., Yamboliev, I., Duan, D., and Hume, J. R. (2003) Functional effects of novel anti-ClC-3 antibodies on native volume-sensitive osmolyte and anion channels in cardiac and smooth muscle cells. *Am. J. Physiol.* **285,** H1453–H1463
41. Wen, H., Nagelhus, E. A., Amiry-Moghaddam, M., Agre, P., Ottersen, O. P., and Nielsen, S. (1999) Ontogeny of water transport in rat brain: postnatal expression of the aquaporin-4 water channel. *Eur. J. Neurosci.* **11,** 935–945
42. Taniguchi, M., Yamashita, T., Kumura, E., Tamatani, M., Kobayashi, A., Yokawa, T., Maruno, M., Kato, A., Ohnishi, T., Kohmura, E., et al. (2000) Induction of aquaporin-4 water channel mRNA after focal cerebral ischemia in rat. *Brain Res. Mol.* **78,** 131–137
43. Manley, G. T., Fujimura, M., Ma, T., Noshita, N., Filiz, F., Bollen, A. W., Chan, P., and Verkman, A. S. (2000) Aquaporin-4 deletion in mice reduces brain edema after acute water intoxication and ischemic stroke. *Nat. Med.* **6,** 159–163
44. Nico, B., Frigeri, A., Nicchia, G. P., Quondamatteo, F., Herken, R., Errede, M., Ribatti, D., Svelto, M., and Roncali, L. (2001) Role of aquaporin-4 water channel in the development and integrity of the blood-brain barrier. *J. Cell Sci.* **114,** 1297–1307
45. Venero, J. L., Vizuete, M. L., Machado, A., and Cano, J. (2001) Aquaporins in the central nervous system. *Prog. Neurobiol.* **63,** 321–336
46. Badaut, J., Lasbennes, F., Magistretti, P. J., and Regli, L. (2002) Aquaporins in brain: distribution, physiology, and pathophysiology. *J. Cereb. Blood Flow Metab.* **22,** 367–378
47. Le Bihan, D., and van Zijl, P. C. M., Eds. (2002) Diffusion tensor imaging and axonal mapping—state of the art. *NMR Biomed.* **15,** 431–593
48. McDaniel, B., Sheng, H. X., Warner, D. S., Hedlund, L. W., and Benveniste, H. (2001) Tracking brain volume changes in C57BL/6J and ApoE-deficient mice in a model of neurodegeneration: A 5-week longitudinal micro-MRI study. *Neuroimage* **14,** 1244–1255
49. Beeri, R., Le Novere, N., Mervis, R., Huberman, T., Grauer, E., Changeux, J. P., and Soreq, H. (1997) Enhanced hemicholinium binding and attenuated dendrite branching in cognitively impaired acetylcholinesterase-transgenic mice. *J. Neurochem.* **69,** 2441–2451
50. Lu, H., and Sun, S. Q. (2003) A correlative study between AQP4 expression and the manifestation of DWI after the acute ischemic brain edema in rats. *Chin. Med. J. (Engl.)* **116,** 1063–1069
51. Vajda, Z., Pedersen, M., Fuchtbauer, E. M., Wertz, K., Stodkilde-Jorgensen, H., Sulyok, E., Doczi, T., Neely, J. D., Agre, P., Frokiaer, J., et al. (2002) Delayed onset of brain edema and mislocalization of aquaporin-4 in dystrophin-null transgenic mice. *Proc. Natl. Acad. Sci. USA* **99,** 13131–13136
52. Grauer, E., Ben Nathan, D., Lustig, S., Kobiler, D., Kapon, J., and Danenberg, H. D. (2001) Viral neuroinvasion as a marker for BBB integrity following exposure to cholinesterase inhibitors. *Life Sci.* **68,** 985–990
53. Tracey, K. J. (2002) The inflammatory reflex. *Nature* **420,** 853–859
54. Abbott, N. J. (2002) Astrocyte-endothelial interactions and blood-brain barrier permeability. *J. Anat.* **200,** 629–638
55. Mirjany, M., Ho, L., and Pasinetti, G. M. (2002) Role of cyclooxygenase-2 in neuronal cell cycle activity and glutamate-mediated excitotoxicity. *J. Pharmacol. Exp. Ther.* **301,** 494–500
56. Vizuete, M. L., Venero, J. L., Vargas, C., Ilundain, A. A., Echevarria, M., Machado, A., and Cano, J. (1999) Differential upregulation of aquaporin-4 mRNA expression in reactive astrocytes after brain injury: potential role in brain edema. *Neurobiol. Dis.* **6,** 245–258
57. Chen, Y., Ruetzler, C., Pandipati, S., Spatz, M., McCarron, R. M., Becker, K., and Hallenbeck, J. M. (2003) Mucosal tolerance to E-selectin provides cell-mediated protection against ischemic brain injury. *Proc. Natl. Acad. Sci. USA*
58. Zhang, Z. G., Tsang, W., Zhang, L., Powers, C., and Chopp, M. (2001) Up-regulation of neuropilin-1 in neovasculature after focal cerebral ischemia in the adult rat. *J. Cereb. Blood Flow Metab.* **21,** 541–549
59. Cho, H., Shimazaki, K., Takeuchi, K., Kobayashi, S., Watanabe, K., Oguro, K., Masuzawa, T., and Kawai, N. (1998) Biphasic changes in F3/contactin expression in the gerbil hippocampus after transient ischemia. *Exp. Brain Res.* **122,** 227–234
60. Omori, N., Jin, G., Li, F., Zhang, W. R., Wang, S. J., Hamakawa, Y., Nagano, I., Manabe, Y., Shoji, M., and Abe, K. (2002) Enhanced phosphorylation of PTEN in rat brain after transient middle cerebral artery occlusion. *Brain Res.* **954,** 317–322
61. Franklin, K. B. J., and Paxinos, G. (2001) *The Mouse Brain in Sterotaxic Coordinates*, Academic Press, San Diego
62. Birikh, K. R., Sklan, E. H., Shoham, S., and Soreq, H. (2003) Interaction of "readthrough" acetylcholinesterase with RACK1 and PKCbeta II correlates with intensified fear-induced conflict behavior. *Proc. Natl. Acad. Sci. USA* **100,** 283–288

Received for publication August 22, 2004.
Accepted for publication February 8, 2005.